



# Numerical solutions of the Allen–Cahn equation with the $p$ -Laplacian



Dongsun Lee<sup>a</sup>, Chaeyoung Lee<sup>b,\*</sup>

<sup>a</sup> Department of Mathematics Education, Incheon National University, Incheon 21999, Republic of Korea

<sup>b</sup> Department of Mathematics, Korea University, Seoul 02841, Republic of Korea

## ARTICLE INFO

### Article history:

Received 7 March 2022

Revised 4 July 2022

Accepted 19 July 2022

Available online 7 August 2022

### Keywords:

$p$ -Laplacian Operator

Finite differences

Allen–Cahn equation

Boundedness of solution

Discrete energy dissipation

## ABSTRACT

We investigate the behavior of the numerical solutions of the  $p$ -Laplacian Allen–Cahn equation. Because of the  $p$ -Laplacian's challenging numerical properties, many different methods have been proposed for the discretized  $p$ -Laplacian. In this paper, we provide and analyze a numerical scheme for the boundedness of solutions and energy decay properties. For a comprehensive understanding of the effect of  $p$ -Laplacian and its relationship in the context of phase-field modeling, we compare the temporal evolution and compute the eigenpairs of the classical, fractional, and  $p$ -Laplacian in the Allen–Cahn equations. As for the  $p$ -Laplacian Allen–Cahn equation, we characterize different morphological changes of numerical solutions under various numerical tests such as phase separation, equilibrium profile, boundedness of solution, energy decay, traveling wave solution, geometric motions, and comparison of the Allen–Cahn equations with the three different Laplacians. Our results imply that the interface profile along the two-phase boundary lines changes more steeply than classical one as the  $p$  order decreases, therefore, the  $p$ -Laplacian Allen–Cahn equation can be applied for the description of phase interface where it is important to maintain sharply.

© 2022 Elsevier Inc. All rights reserved.

## 1. Introduction

The  $p$ -Laplacian has been studied intensively in the past few decades [1–5,27]. There has also been a surge of interest in the  $p$ -Laplacian in many different contexts from game theory to dynamical systems, machine learning, and image processing. In [6], a generalized spectral clustering using the  $p$ -Laplacian was proposed and its advantages were shown through numerical experiments according to the value of  $p$ . In [7], several applications of image processing and machine learning were presented by using the  $p$ -Laplacian equation. In [8], a nonlinear diffusion equation with the  $p$ -Laplacian was introduced for networks. In [9], the discrete  $p$ -Laplacian, combined with the nonlinear Cucker–Smale model, was adopted to model the semi-noflocking phenomenon. Here, they aimed at the slow dispersion of particles, and their works implied that particles can be organized into ordered motion. In [10], the authors presented the system for the process of coral fertilization under the influence of chemotaxis and investigated the interaction among  $p$ -Laplacian diffusion, chemotaxis cross diffusion, and the fluid dynamic mechanism. In [11], a phase-field model that involves the  $p$ -Laplacian was studied using a finite element approximation. In [12], the authors considered a generalized Kelvin–Voigt equation involving  $p$ -Laplacian and damping

\* Corresponding author.

E-mail addresses: [esen@inu.ac.kr](mailto:esen@inu.ac.kr) (D. Lee), [chae1228@korea.ac.kr](mailto:chae1228@korea.ac.kr) (C. Lee).

term. The original equation describes a vibration isolator with viscoelasticity. In [13], nonlinear elliptic equations with the  $p$ -Laplacian is numerically solved using a second-order-in-time scheme [14].

We define the  $p$ -Laplacian as

$$\Delta_p u = \nabla \cdot \left( |\nabla u|^{p-1} \frac{\nabla u}{|\nabla u|} \right).$$

Here,  $p$  is allowed to range over  $1 \leq p \leq 2$ . The gradient of  $u$  in a two-dimensional (2D) domain and its magnitude are respectively

$$\nabla u(x, y) = \left( \frac{\partial u}{\partial x}, \frac{\partial u}{\partial y} \right) \quad \text{and} \quad |\nabla u(x, y)| = \sqrt{\left( \frac{\partial u}{\partial x} \right)^2 + \left( \frac{\partial u}{\partial y} \right)^2}.$$

The  $p$ -Laplacian appears in many mathematical models of physical processes such as nonlinear diffusion. For example, let us consider the Allen–Cahn (AC) equation with the  $p$ -Laplacian. The classical AC equation, i.e.,  $p = 2$  under the Neumann boundary condition has been intensively studied. It was originally introduced to model the motion of anti-phase domain coarsening in a binary alloy [15]. The equation has been widely used for applications such as image processing [16], crystal growth [17], and so on, based on its representative property dynamics like motion by mean curvature [18,19]. However, few of these studies have dealt with the  $p$ -Laplacian operator. Moreover, since solving highly nonlinear terms is still challenging, there is a need to develop more accurate and efficient numerical schemes for the nonlinear equations with the  $p$ -Laplacian operator, such as unconditionally energy stable [20–23], second- order backward differentiation formula (BDF2) [24], scalar auxiliary variable (SAV) schemes [25,26].

Together with the  $p$ -Laplacian operator, the  $p$ -Laplacian AC equation ( $p$ -AC equation) is given by

$$\frac{du}{dt} = \epsilon \Delta_p u + \frac{1}{\epsilon} (u - u^3) = \epsilon \nabla \cdot \left( |\nabla u|^{p-1} \frac{\nabla u}{|\nabla u|} \right) + \frac{1}{\epsilon} (u - u^3). \quad (1)$$

If exponent  $p = 1$ , the  $p$ -Laplacian becomes the mean curvature operator  $H$ :

$$\Delta_1 = \nabla \cdot \left( \frac{\nabla u}{|\nabla u|} \right) = -H.$$

Note that the mean curvature operator  $H$  in 2D space can be expressed by

$$H = \frac{u_y^2 u_{xx} - 2u_x u_y u_{xy} + u_x^2 u_{yy}}{(u_x^2 + u_y^2)^{\frac{3}{2}}}.$$

According to  $p$  values, it is expected that the interfacial dynamics will be different.

The main purpose of this paper is to investigate the dynamics of the numerical solutions of the  $p$ -AC equation. Moreover, we would like to provide details of how the type of Laplacians influences a solution to the AC equation. The contents of this paper are as follows. Section 2 presents the discretization for the  $p$ -AC equation and analysis of the basic properties. To demonstrate the dynamics of the  $p$ -AC equation, a variety of numerical simulations are conducted in Section 3. Moreover, we compare the dynamics and eigenvalues among the  $p$ -Laplacian, fractional Laplacian, and classical Laplacian in the AC equation. Finally, the conclusions are given in Section 4.

## 2. Discretization of the Allen–Cahn equations with the $p$ -Laplacian

The numerical dynamics of the AC equation, i.e., for  $p = 2$  has been studied extensively in much literature. In this work, we consider the  $p$ -Laplacian  $-\Delta_p$  with the Neumann boundary conditions instead of the classical Neumann-Laplacian  $-\Delta$  in the AC equation. The  $p$ -Laplacian depending on  $p$  is known that the operator has a nonlinear property, however, its numerical character in the AC equation has been less studied by now.

### 2.1. Discretization for the computation

Note that we consider the 2D case only. The 1D and 3D cases can be dealt with in the same fashion. We first discretize continuous variables. In a 2D space  $\Omega = (x_a, x_b) \times (y_a, y_b)$ , for positive integers  $N_x$  and  $N_y$ , let the uniform space step size

be  $h = (x_b - x_a)/N_x = (y_b - y_a)/N_y$  and the temporal step size be  $\Delta t$ . The numerical solution at  $(x_i, y_j, t_n)$  is defined as  $u_{i,j}^k$ , where a cell-centered point in a discrete domain  $\Omega_h$  is  $(x_i, y_j) = (x_a + (i - 0.5)h, y_a + (j - 0.5)h)$  for  $1 \leq i \leq N_x$ ,  $1 \leq j \leq N_y$  and the time is  $t_n = k\Delta t$  for a positive integer  $k$ . For simplicity, assume that  $x_a = y_a$ ,  $x_b = y_b$ , and  $N = N_x = N_y$ . The discrete gradient operators and divergence operator are

$$\begin{aligned}\nabla_h u_{i+\frac{1}{2},j}^k &= \frac{(u_{i+1,j}^k - u_{i,j}^k)}{h}, \quad \nabla_h u_{i-\frac{1}{2},j}^k = \frac{(u_{i,j}^k - u_{i-1,j}^k)}{h}, \\ \nabla_h u_{i,j+\frac{1}{2}}^k &= \frac{(u_{i,j+1}^k - u_{i,j}^k)}{h}, \quad \nabla_h u_{i,j-\frac{1}{2}}^k = \frac{(u_{i,j}^k - u_{i,j-1}^k)}{h}, \\ |\nabla_h u_{i+\frac{1}{2},j}^k|^p &= \left[ \frac{(u_{i+1,j}^k - u_{i,j}^k)^2}{h^2} + \frac{(u_{i,j+1}^k - u_{i,j-1}^k)^2}{4h^2} \right]^{p/2}, \\ |\nabla_h u_{i,j+\frac{1}{2}}^k|^p &= \left[ \frac{(u_{i+1,j}^k - u_{i-1,j}^k)^2}{4h^2} + \frac{(u_{i,j+1}^k - u_{i,j}^k)^2}{h^2} \right]^{p/2}, \\ \text{and } \nabla_h \cdot (u_{i,j}^k, v_{i,j}^k) &= \frac{\left( u_{i+\frac{1}{2},j}^k - u_{i-\frac{1}{2},j}^k + v_{i,j+\frac{1}{2}}^k - v_{i,j-\frac{1}{2}}^k \right)}{h},\end{aligned}$$

where the homogeneous Neumann boundary condition is imposed. In addition, the discrete magnitude of  $p$ -gradient, and  $p$ -Laplacian are

$$\begin{aligned}\Delta_{p,h} u_{i,j}^k &= \nabla_h \cdot (|\nabla_h u_{i,j}^k|^{p-2} \nabla_h u_{i,j}^k) \\ &= \frac{\left| \nabla_h u_{i+\frac{1}{2},j}^k \right|^{p-2} \nabla_h u_{i+\frac{1}{2},j}^k - \left| \nabla_h u_{i-\frac{1}{2},j}^k \right|^{p-2} \nabla_h u_{i-\frac{1}{2},j}^k + \left| \nabla_h u_{i,j+\frac{1}{2}}^k \right|^{p-2} \nabla_h u_{i,j+\frac{1}{2}}^k - \left| \nabla_h u_{i,j-\frac{1}{2}}^k \right|^{p-2} \nabla_h u_{i,j-\frac{1}{2}}^k}{h} \\ &= \frac{\left| \nabla_h u_{i+\frac{1}{2},j}^k \right|^{p-2} u_{i+1,j}^k + \left| \nabla_h u_{i-\frac{1}{2},j}^k \right|^{p-2} u_{i-1,j}^k + \left| \nabla_h u_{i,j+\frac{1}{2}}^k \right|^{p-2} u_{i,j+1}^k + \left| \nabla_h u_{i,j-\frac{1}{2}}^k \right|^{p-2} u_{i,j-1}^k}{h^2} \\ &\quad - \frac{\left( \left| \nabla_h u_{i+\frac{1}{2},j}^k \right|^{p-2} + \left| \nabla_h u_{i-\frac{1}{2},j}^k \right|^{p-2} + \left| \nabla_h u_{i,j+\frac{1}{2}}^k \right|^{p-2} + \left| \nabla_h u_{i,j-\frac{1}{2}}^k \right|^{p-2} \right) u_{i,j}^k}{h^2}.\end{aligned}$$

We denote by  $u^k$ , and  $\nabla_h u^k$  the discrete values at the  $k$ -th temporal step, i.e.,

$$u^k = \{u_{i,j}^k, 1 \leq i, j \leq N\}, \quad \text{and } \nabla_h u^k = \left\{ \left( \nabla_h u_{i+\frac{1}{2},j}^k, \nabla_h u_{i,j+\frac{1}{2}}^k \right) = \nabla_h u_{i+N(j-1)}^k = \nabla_h u_{i,j}^k, 1 \leq i, j \leq N \right\}.$$

Also, we define the discrete inner product as follows:

$$\langle u, v \rangle = \sum_{i=1, j=1}^N u_{i,j} v_{i,j}, \quad \text{and } \langle \nabla u, \nabla v \rangle = \sum_{i=1}^{N-1} \sum_{j=1}^N \nabla_h u_{i+\frac{1}{2},j} \nabla_h v_{i+\frac{1}{2},j} + \sum_{i=1}^N \sum_{j=1}^{N-1} \nabla_h u_{i,j+\frac{1}{2}} \nabla_h v_{i,j+\frac{1}{2}}.$$

Furthermore, we define the discrete Laplacian by

$$\Delta u_{i,j} = \frac{u_{i-1,j} + u_{i+1,j} + u_{i,j-1} + u_{i,j+1} - 4u_{i,j}}{h^2}.$$

With the discrete Laplacian operator, the notation  $\Delta u$  can be represented by

$$\Delta u := \{ \Delta u_{i,j}, 1 \leq i, j \leq N \}.$$

## 2.2. Analysis of basic properties of the $p$ -AC equation

**Proposition 1.** *With the discrete gradient  $\nabla$  and Laplacian  $\Delta$  operators, we can derive the summation by parts:*

$$\langle -\Delta_{p,h} u, v \rangle = \langle |\nabla u|^{p-2} \nabla u, \nabla v \rangle.$$

**Proof.** We consider the following computation:

$$\begin{aligned} \langle |\nabla u|^{p-2} \nabla u, \nabla v \rangle &= \sum_{i=1}^{N-1} \sum_{j=1}^N |\nabla_h u_{i+\frac{1}{2}, j}|^{p-2} \left( \frac{u_{i+1, j} - u_{i, j}}{h} \right) \left( \frac{v_{i+1, j} - v_{i, j}}{h} \right) \\ &\quad + \sum_{i=1}^N \sum_{j=1}^{N-1} |\nabla_h u_{i, j+\frac{1}{2}}|^{p-2} \left( \frac{u_{i, j+1} - u_{i, j}}{h} \right) \left( \frac{v_{i, j+1} - v_{i, j}}{h} \right) \\ &= \frac{1}{h^2} \sum_{i=1}^{N-1} \sum_{j=1}^N |\nabla_h u_{i+\frac{1}{2}, j}|^{p-2} (u_{i+1, j} - u_{i, j})(v_{i+1, j} - v_{i, j}) \\ &\quad + \frac{1}{h^2} \sum_{i=1}^N \sum_{j=1}^{N-1} |\nabla_h u_{i, j+\frac{1}{2}}|^{p-2} (u_{i, j+1} - u_{i, j})(v_{i, j+1} - v_{i, j}). \end{aligned}$$

With the help of the boundary conditions, we set  $u_{N+1, j} = u_{N, j}$ ,  $u_{0, j} = u_{1, j}$  and  $u_{i, N+1} = u_{i, N}$ ,  $u_{i, 0} = u_{i, 1}$  for  $1 \leq i, j \leq N$ . It readily tells us that

$$\begin{aligned} &\frac{1}{h^2} \sum_{i=0}^N \sum_{j=0}^N |\nabla_h u_{i+\frac{1}{2}, j}|^{p-2} [(u_{i+1, j} v_{i+1, j} - u_{i, j} v_{i+1, j}) - (u_{i+1, j} v_{i, j} - u_{i, j} v_{i, j})] \\ &\quad + \frac{1}{h^2} \sum_{i=0}^N \sum_{j=0}^N |\nabla_h u_{i, j+\frac{1}{2}}|^{p-2} [(u_{i, j+1} v_{i, j+1} - u_{i, j} v_{i, j+1}) - (u_{i, j+1} v_{i, j} - u_{i, j} v_{i, j})] \\ &= \frac{1}{h^2} \left( \sum_{i=1}^{N+1} \sum_{j=0}^N |\nabla_h u_{i-\frac{1}{2}, j}|^{p-2} u_{i, j} v_{i, j} - \frac{1}{h^2} \sum_{i=1}^{N+1} \sum_{j=0}^N |\nabla_h u_{i-\frac{1}{2}, j}|^{p-2} u_{i-1, j} v_{i, j} - \sum_{i=0}^N \sum_{j=0}^N |\nabla_h u_{i+\frac{1}{2}, j}|^{p-2} u_{i+1, j} v_{i, j} \right. \\ &\quad \left. + \sum_{i=0}^N \sum_{j=0}^N |\nabla_h u_{i+\frac{1}{2}, j}|^{p-2} u_{i, j} v_{i, j} + \sum_{i=0}^N \sum_{j=1}^{N+1} |\nabla_h u_{i, j-\frac{1}{2}}|^{p-2} u_{i, j} v_{i, j} - \sum_{i=0}^N \sum_{j=1}^{N+1} |\nabla_h u_{i, j-\frac{1}{2}}|^{p-2} u_{i, j-1} v_{i, j} \right. \\ &\quad \left. - \sum_{i=0}^N \sum_{j=0}^N |\nabla_h u_{i, j+\frac{1}{2}}|^{p-2} u_{i, j+1} v_{i, j} + \sum_{i=0}^N \sum_{j=0}^N |\nabla_h u_{i, j+\frac{1}{2}}|^{p-2} u_{i, j} v_{i, j} \right) \\ &= \frac{1}{h} \sum_{i=1}^N \sum_{j=1}^N \left[ \frac{(|\nabla_h u_{i-\frac{1}{2}, j}|^{p-2} u_{i, j} - |\nabla_h u_{i-\frac{1}{2}, j}|^{p-2} u_{i-1, j})}{h} - \frac{(|\nabla_h u_{i+\frac{1}{2}, j}|^{p-2} u_{i+1, j} - |\nabla_h u_{i+\frac{1}{2}, j}|^{p-2} u_{i, j})}{h} \right. \\ &\quad \left. + \frac{(|\nabla_h u_{i, j-\frac{1}{2}}|^{p-2} u_{i, j} - |\nabla_h u_{i, j-\frac{1}{2}}|^{p-2} u_{i, j-1})}{h} - \frac{(|\nabla_h u_{i, j+\frac{1}{2}}|^{p-2} u_{i, j+1} - |\nabla_h u_{i, j+\frac{1}{2}}|^{p-2} u_{i, j})}{h} \right] v_{i, j} \\ &= \langle \nabla \cdot (|\nabla_h u|^{p-2} \nabla u), v \rangle = \langle -\Delta_{p, h} u, v \rangle. \end{aligned}$$

□

The  $p$ -Laplacian is derived from a functional given  $F(u) : \mathbb{R}^{N^2} \rightarrow \mathbb{R}$  by

$$F(u) := \frac{1}{p} \langle |\nabla u|^p, \mathbf{1} \rangle, \tag{2}$$

where  $N$  is a positive integer and  $\mathbf{1} = (1, 1, \dots, 1) \in \mathbb{R}^{N^2}$ . When  $p = 1$ , minimizing the above functional leads to the mean curvature operator, i.e., it turns out that Eq. (2) is total variation functional. Note that the 2D discrete  $l_\infty$ -norm is defined as  $\|u\|_\infty = \max_{1 \leq i, j \leq N} |u_{i, j}|$  and the 2D discrete  $l_2$ -norm as  $\|u\|_2 = \sqrt{\sum_{i=1}^N \sum_{j=1}^N |u_{i, j}|^2}$ .

We consider the explicit Euler's method to solve the governing Eq. (1) numerically:

$$\frac{u_{i, j}^{k+1} - u_{i, j}^k}{\Delta t} = \epsilon \Delta_{p, h} u_{i, j}^k + \frac{1}{\epsilon} (u_{i, j}^k - (u_{i, j}^k)^3). \tag{3}$$

**Theorem 2.** Let  $\lambda_u = 4/h^2 > 0$  be the largest eigenvalue for the classical Neumann-Laplacian  $-\Delta_h u = \lambda_u u$ . Suppose that  $\|u\|_\infty = u_{\max}$ , where  $1 < u_{\max}$ . Then, the  $p$ -Laplacian  $-\Delta_{p, h}$  is positive semi-definite. Moreover, the largest eigenvalue of  $-\Delta_{p, h}$  is bounded by  $2^p h^{-p}$ .

**Proof.** Due to  $p > 0$  and Neumann boundary conditions, it is readily seen that

$$0 \leq F(u) = \frac{1}{p} \left\langle |\nabla u|^p, \mathbf{1} \right\rangle = \frac{1}{p} \left\langle |\nabla u|^{p-2} \nabla u, \nabla u \right\rangle = \frac{1}{p} \left\langle \nabla \cdot (-|\nabla u|^{p-2} \nabla u), u \right\rangle = \frac{1}{p} \left\langle -\Delta_{p,h} u, u \right\rangle \text{ for all } u \in \mathbb{R}^{N^2}.$$

Together with the operator  $-\Delta_h$ , which satisfies  $-\Delta_h u = \lambda_u u$ , we have

$$0 \leq \frac{\langle u, -\Delta_{p,h} u \rangle}{\|u\|_2^2} = \frac{\langle \nabla \cdot (-|\nabla u|^{p-2} \nabla u), u \rangle}{\|u\|_2^2} \leq |\nabla u|^{p-2} \frac{\langle \Delta_h u, u \rangle}{\|u\|_2^2} \leq \left( \frac{2u_{\max}}{h} \right)^{p-2} \lambda_u = \frac{2^p (u_{\max})^{p-2}}{h^p}.$$

Using mathematical induction on  $k$ , we show the boundedness of the numerical solution  $u^{k+1}$ .  $\square$

**Theorem 3.** Let  $\epsilon = m\Delta t$ , and  $m$  be a positive integer such that  $m \geq 2$ . We set  $\Delta t > 0$  and  $m$  to have

$$\beta + \frac{\beta - \beta^3}{m} \leq \left( 1 - m \frac{2^p (\Delta t)^2}{h^p} \right) u_{\max},$$

where we define  $\beta := \sqrt{(1+m)/3} \leq u_{\max}$ . Recall that  $u_{\max} > 1$ . Suppose that  $\{u^k\}$  is the numerical solution generated by the numerical scheme (3). For all  $k \geq 0$ , the numerical solution  $u^{k+1}$  has the boundedness property. We set an initial  $u^0$  to have  $\|u^0\|_\infty \leq u_{\max}$ .

**Proof.** It suffices to show that  $\|u^k\|_\infty \leq u_{\max}$  implies  $\|u^{k+1}\|_\infty \leq u_{\max}$ . To see that, we consider the following inequalities:

$$\| -\Delta_{p,h} u^k \|_\infty = \max_i \left( \left| \sum_j^{N^2} -\Delta_{p,h} u_{i,j}^k \right| \right) \leq \| -\Delta_{p,h} u^k \|_2 \leq \frac{2^p (u_{\max})^{p-2}}{h^p}.$$

The last inequality follows from Theorem 2. We define  $f$  on  $[-u_{\max}, u_{\max}]$  by

$$f(x) := x + \frac{1}{m} (x - x^3).$$

The function  $f$  is strictly increasing on  $[-u_{\max}, u_{\max}]$  since it has extreme values at  $-\beta$  and  $\beta$ . Especially,  $f$  attains the maximum  $\beta + (\beta - \beta^3)/m$  and minimum  $-\beta + (\beta^3 + \beta)/m$ . Due to the assumption on  $\Delta t$ ,  $m$  and  $(u_{\max})^{p-2} \leq u_{\max}$ , we get

$$\begin{aligned} \beta + \frac{\beta - \beta^3}{m} &\leq \left( 1 - m \frac{2^p (\Delta t)^2}{h^p} \right) u_{\max} \\ m(\Delta t)^2 \frac{2^p (u_{\max})^{p-2}}{h^p} + \beta + \frac{\beta - \beta^3}{m} &\leq u_{\max} \end{aligned}$$

This implies that

$$\|u_{i,j}^{k+1}\|_\infty = \left\| u_{i,j}^k + \epsilon \Delta t \Delta_{p,h} u_{i,j}^k + \frac{\Delta t}{\epsilon} (u_{i,j}^k - (u_{i,j}^k)^3) \right\|_\infty \leq u_{\max}.$$

$\square$

Given  $\epsilon$  and  $p$ , we define a discrete functional  $\mathcal{E}_{\epsilon,p} : \mathbb{R}^{N^2} \rightarrow \mathbb{R}$  by

$$\mathcal{E}_{\epsilon,p}(u) := \frac{\epsilon}{2} \left\langle |\nabla u|^{p/2}, |\nabla u|^{p/2} \right\rangle + \frac{1}{4\epsilon} \left\langle (u^2 - \mathbf{1}), (u^2 - \mathbf{1}) \right\rangle. \quad (4)$$

Since  $u$  is bounded, we can define  $M$  in such a way that  $M := \max |\nabla u|$ .

**Theorem 4.** Let us set  $\Delta t$  such that  $\frac{(3M-1)}{8\epsilon} + \frac{8M}{h^2} \leq \frac{1}{\Delta t}$ . Then, our proposed scheme decreases the discrete functional  $\mathcal{E}_{\epsilon,p}$ .

**Proof.** With  $u^{k+1}$ ,  $u^k$  and  $M$ , we can obtain

$$\begin{aligned} &\langle |\nabla u^{k+1}|^{p/2}, |\nabla u^{k+1}|^{p/2} \rangle - \langle |\nabla u^k|^{p/2}, |\nabla u^k|^{p/2} \rangle \\ &= 2 \langle \nabla u^{k+1}, |\nabla u^k|^{p-2} \nabla u^k \rangle - 2 \langle \nabla u^k, |\nabla u^k|^{p-2} \nabla u^k \rangle + \langle \nabla u^{k+1}, |\nabla u^{k+1}|^{p-2} \nabla u^{k+1} \rangle + \langle \nabla u^k, |\nabla u^k|^{p-2} \nabla u^k \rangle \\ &\quad - 2 \langle \nabla u^{k+1}, |\nabla u^k|^{p-2} \nabla u^k \rangle \\ &\leq 2 \langle \nabla u^{k+1} - \nabla u^k, |\nabla u^k|^{p-1} \frac{\nabla u^k}{|\nabla u^k|} \rangle + M \langle \nabla u^{k+1} - \nabla u^k, \nabla u^{k+1} - \nabla u^k \rangle \\ &\leq 2 \langle u^{k+1} - u^k, -\nabla \cdot \left( |\nabla u^k|^{p-1} \frac{\nabla u^k}{|\nabla u^k|} \right) \rangle + \frac{8M}{h^2} \langle u^{k+1} - u^k, u^{k+1} - u^k \rangle. \end{aligned}$$

By the Taylor expansion, we have

$$\begin{aligned}
\mathcal{E}_{\epsilon,p}(u^{k+1}) - \mathcal{E}_{\epsilon,p}(u^k) &= \frac{\epsilon}{2} (\langle |\nabla u^{k+1}|^{p/2}, |\nabla u^{k+1}|^{p/2} \rangle - \langle |\nabla u^k|^{p/2}, |\nabla u^k|^{p/2} \rangle) \\
&\quad + \frac{1}{4\epsilon} (\langle ((u^{k+1})^2 - \mathbf{1}), ((u^{k+1})^2 - \mathbf{1}) \rangle - \langle ((u^k)^2 - \mathbf{1}), ((u^k)^2 - \mathbf{1}) \rangle) \\
&\leq \langle u^{k+1} - u^k, -\epsilon \nabla \cdot \left( |\nabla u^k|^{p-1} \frac{\nabla u^k}{|\nabla u^k|} \right) \rangle + \frac{8M}{h^2} \|u^{k+1} - u^k\|^2 \\
&\quad + \frac{1}{\epsilon} \langle u^{k+1} - u^k, (u^{k+1})^3 - u^k \rangle + \frac{1}{8\epsilon} (u^{k+1} - u^k)^T (3 \operatorname{diag}(\xi^2) - I) (u^{k+1} - u^k) \\
&\leq -\frac{1}{\Delta t} \langle u^{k+1} - u^k, (u^{k+1} - u^k) \rangle + \frac{8M}{h^2} \|u^{k+1} - u^k\|^2 + \frac{(3M-1)}{8\epsilon} \|u^{k+1} - u^k\|^2 \\
&\leq \left( \frac{(3M-1)}{8\epsilon} + \frac{8M}{h^2} - \frac{1}{\Delta t} \right) \|u^{k+1} - u^k\|^2 \leq 0.
\end{aligned}$$

□

### 3. Numerical simulations

We demonstrate numerical experiments to validate as well as to present the interesting dynamics from our numerical scheme. To begin with, we present the effects of phase separation induced by the nonlinear term in the AC equation. Then, we observe the difference of equilibrium profile when it reaches one of the stable solutions. The boundedness of solutions and energy decay properties are confirmed by numerical tests. Geometric illustration with different  $p$ -orders reveals that the Laplacian with lower  $p$ -order maintains sharp interfaces longer. Moreover, we compare the dynamics of the AC equation with different  $p$ -orders, and observe the differences between the  $p$ -AC and fractional AC equations. It implies that the  $p$ -AC equation generates a sharper interface than the other types of AC equations. The difference is also noticeable from computing the eigenpairs of the  $p$ -Laplacian via the power and gradient descent methods. What is interesting in this experiment is that the  $p$ -Laplacian contains geometrical structures of eigenvectors, which are still similar to the classical ones.

#### 3.1. Phase separation

First, the dynamics of phase separation in binary systems is investigated, which is representative property of the AC equation. For the computational simulation, the parameters are used as  $N = 128$ ,  $h = 1/N$ ,  $\Delta t = 1.0 \times 10^{-4}$ , and  $\epsilon = 1.0 \times 10^{-2}$  on the computational domain  $\Omega = (0, 1)^2$ . The random initial condition is defined as:

$$u(x, y, 0) = 0.2 \operatorname{rand}(x). \quad (5)$$

Note that  $\operatorname{rand}(x)$  is defined as a uniformly distributed random number in the interval  $[-1, 1]$ . Figure 1(a), (b), and (c) show the temporal evolution of Eq. (3) with  $p = 1.2$ ,  $1.6$ , and  $2$ , respectively, until  $t = 1000\Delta t$ .

It can be seen that each morphological change has the coarsening kinetics. All the  $p$ -order AC equation's dynamics share the phenomenon of spinodal decomposition in common, but the lower  $p$ -order slows the dynamics of the coarsening process. In addition to the slowness, the order parameter  $u$  changes steeply across the phase interface.

#### 3.2. Equilibrium profile

Next, the interfacial profiles are compared according to the  $p$  values to closely observe the differences in the transition region at equilibrium. We intend to stop the numerical computations when  $k$ -th and  $(k+1)$ -th iterations meet the criterion

$$\|u^k - u^{k-1}\|_2 < 10^{-5}, \quad (6)$$

where some positive integer  $k \geq 1$ , and define  $u^k$  as a numerical equilibrium solution. The parameters  $N = 128$ ,  $h = 1/N$ ,  $\Delta t = 1.0 \times 10^{-4}$  and  $\epsilon = 2.0 \times 10^{-2}$  are set on the domain  $\Omega = (0, 1)^2$ , and the initial condition is taken as

$$u(x, y, 0) = 0.5 \tanh \left( \frac{x - 0.5}{2\sqrt{2\epsilon}} \right).$$

Figure 2 illustrates the initial condition and numerical equilibrium solutions  $u$  with  $p = 1.2$ ,  $1.6$ , and  $2.0$ . To see the difference of equilibrium solution between  $p$  orders, the cross sections of  $x - u$  at  $y = 0$  are represented. Throughout these results, we verify the relation between the value of  $p$ -order and the interface of AC dynamics, i.e., transition layer structure of connecting  $-1$  and  $1$  is generated in all  $p$ -orders cases, however, its slope is steeper as the positive order  $p$  decreases.

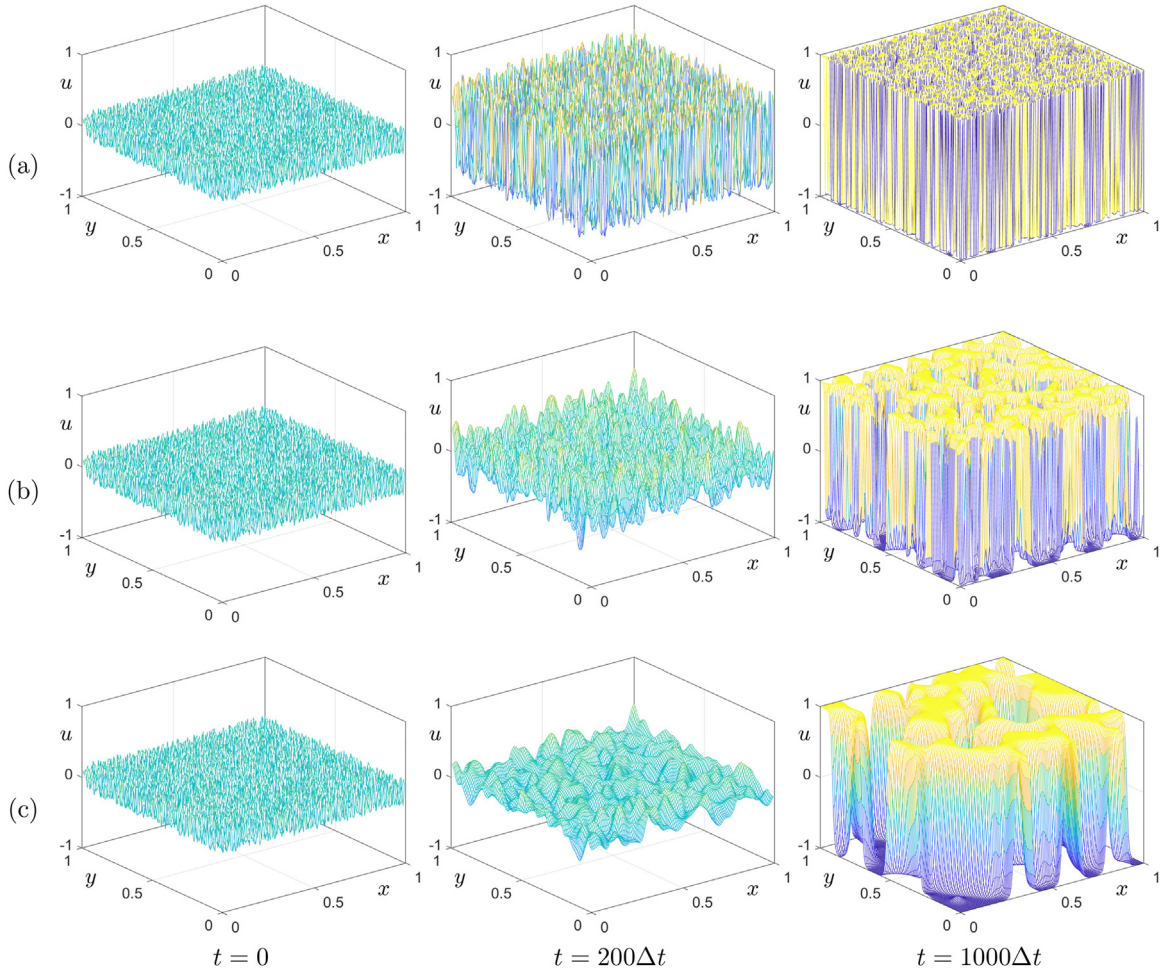


**Fig. 1.** Snapshots with respect to  $p$  values: (a)  $p = 1.2$ , (b)  $p = 1.6$ , and (c)  $p = 2.0$ . Each time is mentioned below each column.

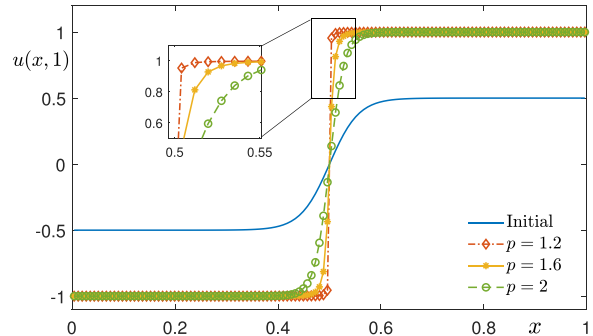


**Fig. 2.** Numerical equilibrium solutions according to  $p$ . Here, we use  $p = 1.2, 1.6$ , and  $2.0$ .

### 3.3. Boundedness

The  $p$ -AC equation also must ensure the boundedness of the solution, i.e., positivity-preserving property. From the numerical aspects, the boundedness of solution is challenging, due to the discretizations of Laplacian. Here, we confirm that the boundedness is valid for our proposed numerical scheme of the  $p$ -AC equation, and justify the boundedness by numerical experiments.

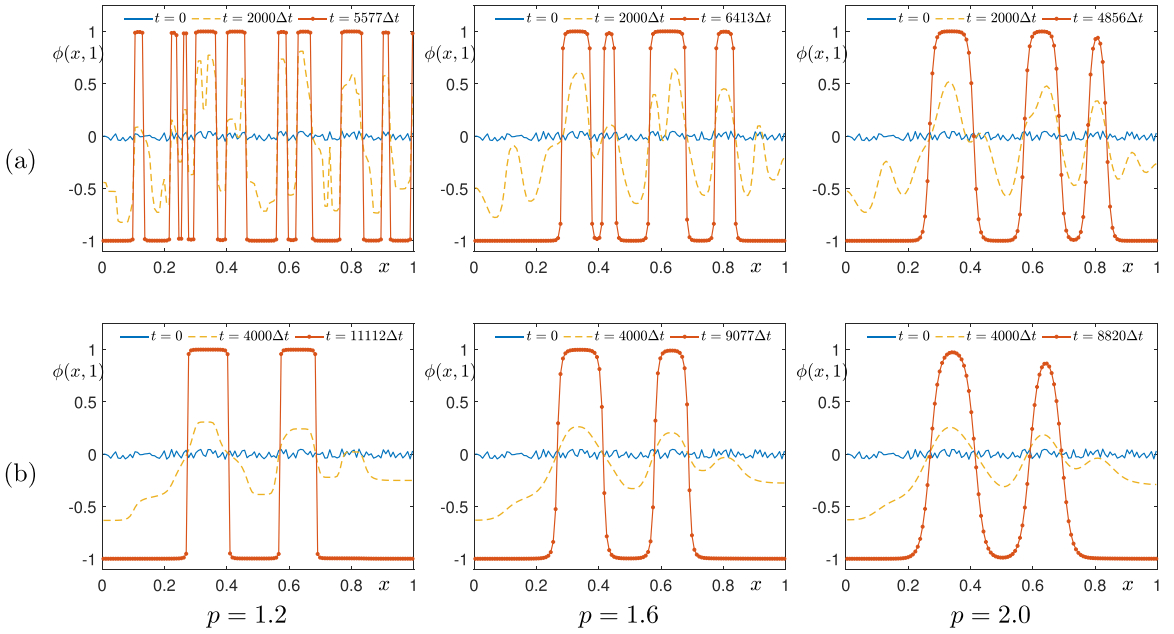


**Fig. 3.** Temporal evolution of numerical solutions driven by  $p$ -Laplacian according to  $\epsilon$  and  $p$  values: (a)  $\epsilon = 0.01$  and (b)  $\epsilon = 0.02$ . From left to right, the values of  $p$  are 1.2, 1.6, and 2.0.

The numerical test is performed to demonstrate the boundedness when the numerical solution approaches the equilibrium state. The parameters are given as  $N = 128$ ,  $h = 1/N$ ,  $\Delta t = 2.0 \times 10^{-5}$  and  $\epsilon = 1.0 \times 10^{-3}$  on the domain  $\Omega = (0, 1)^2$ , and the initial condition is taken as

$$u(x, y, 0) = 0.05 \text{rand}(x). \quad (7)$$

The stopping criterion is the same as Eq. (6). Figure 3 shows the temporal evolution according to  $p$  values. It is observed that the numerical solutions are bounded between  $-1$  and  $1$  regardless of  $p$  values. Numerical results also indicate that the smaller the value of  $p$ , the better the interface is preserved.

### 3.4. Total energy dissipation

In this section, a test is conducted to numerically verify that the total energy functional (4) of the governing equation decreases over time when the proposed scheme is applied. The purpose of this experiment is to see the discrete solutions by all  $p$ -orders decay the discrete total energy. Since we cannot see all  $p$ -orders' evolution, we choose three cases  $p = 1.2$ ,  $p = 1.6$ , and  $p = 2.0$ . The discrete total energy is defined by

$$\mathcal{E}_{\epsilon, p}(u^k) = \frac{h^2 \epsilon}{2} \sum_{i=1}^N \sum_{j=1}^N |\nabla_h u_{i,j}^k|^p + \frac{h^2}{4\epsilon} \sum_{i=1}^N \sum_{j=1}^N [(u_{i,j}^k)^2 - 1]^2.$$

The following parameters are used:  $N = 128$ ,  $h = 1/N$ ,  $\Delta t = 1.0 \times 10^{-4}$ , and  $\epsilon = 5.0 \times 10^{-2}$  on the domain  $\Omega = (0, 1)^2$ , and the initial condition is taken as a square with a center of  $(0.5, 0.5)$  and a side length of 0.25. Figure 4 shows that the discrete total energy is decreasing over time when  $p = 1.2$ , 1.6, and 2.0. The solid lines represent the ratio of the total energy  $\mathcal{E}_{\epsilon, p}(\phi^k)/\mathcal{E}_{\epsilon, p}(\phi^0)$  at  $\Delta t k$ . Each graph (with triangles, stars, and circles) indicates the different evolutions driven by order  $p = 1.2$ ,  $p = 1.6$ , and  $p = 2.0$ . As was expected theoretically, all evolutions preserve the discrete energy dissipation property.

### 3.5. Traveling wave solutions

A traveling wave solution is considered, which is another benchmark problem of the classical AC equation. The traveling wave solution of Eq. (1) with  $p = 2$  is

$$u(x, y, t) = \frac{1}{2} \left( 1 - \tanh \frac{x - 3t/\sqrt{2}}{2\sqrt{2}\epsilon} \right). \quad (8)$$

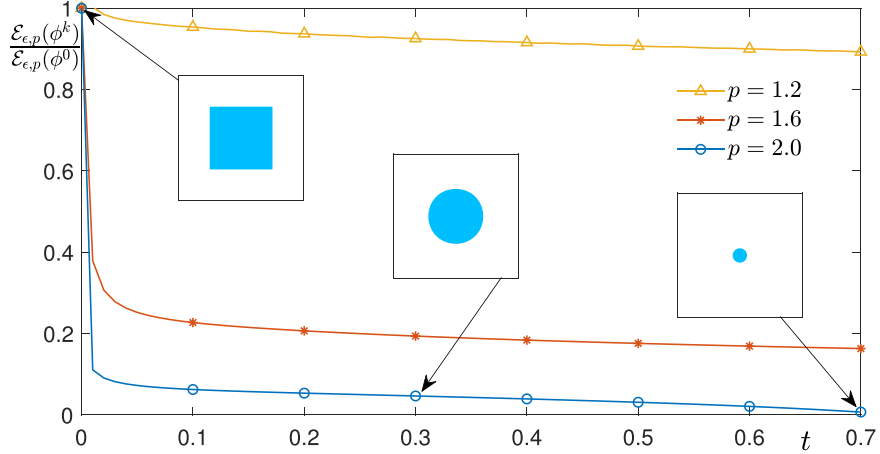


**Fig. 4.** Dissipation of discrete total energy  $\mathcal{E}_{\epsilon,p}(u^k)/\mathcal{E}_{\epsilon,p}(u^0)$  with various  $p$  over time. Here, we used  $p = 1.2$ ,  $1.6$ , and  $2.0$ .

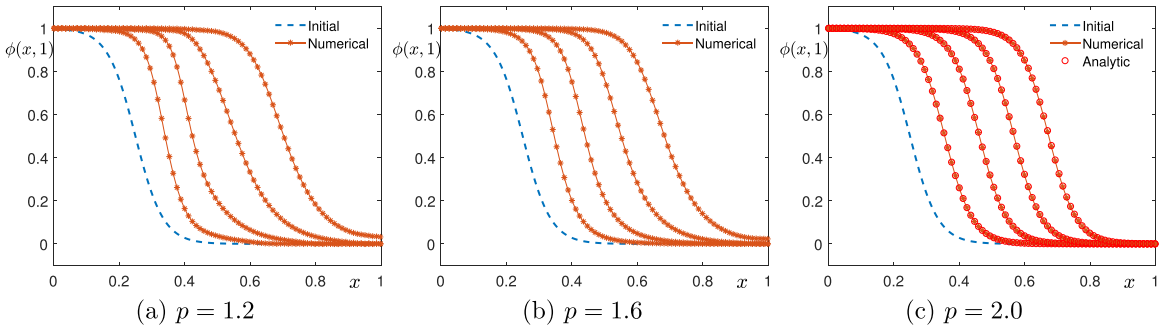


**Fig. 5.** Temporal evolution with (a)  $p = 1.2$ , (b)  $p = 1.6$ , and (c)  $p = 2.0$ .

Note that Eq. (8) is called the analytic solution. The computational domain is  $\Omega = (0, 1)^2$  and the parameters used are  $N = 256$ ,  $h = 1/N$ ,  $\Delta t = 1.0 \times 10^{-4}$ , the final time  $T = 4000\Delta t$ , and  $\epsilon = 3 \times 10^{-2}$ . Figure 5 shows the temporal evolution with respect to  $p$  values when the initial condition is given as

$$u(x, y, 0) = \frac{1}{2} \left( 1 - \tanh \frac{x}{2\sqrt{2}\epsilon} \right).$$

### 3.6. Geometric motions

It is well-known that the zero-level set of a solution of the AC equation follows the curve shortening flow in  $\mathbb{R}^2$ . We test the benchmark example. On the domain  $\Omega = (-1, 1)$ , the parameters used are:  $N = 256$ ,  $h = 2/N$ ,  $\Delta t = 1.0 \times 10^{-4}$ , and  $\epsilon = 1.0 \times 10^{-1}$ , and the initial condition is

$$u(x, y, 0) = \tanh \left( \frac{0.5 + 0.4 \cos(10 \tan^{-1}(y/x)) - \sqrt{x^2 + y^2}}{\sqrt{2}\epsilon} \right). \quad (9)$$

Figure 6(a), (b), and (c) show the temporal evolution of the initial condition (9) with  $p = 1.2$ ,  $1.6$ , and  $2.0$ , respectively. In addition, the comparison among the snapshots with the three different  $p$  is provided in Fig. 6(d)–(e). Here, when  $p = 1.2$ ,  $1.6$ , and  $2.0$ , each time is  $1200\Delta t$ ,  $400\Delta t$ , and  $200\Delta t$ , respectively. It is seen that as  $p$  becomes smaller, the sharp interface is maintained better.

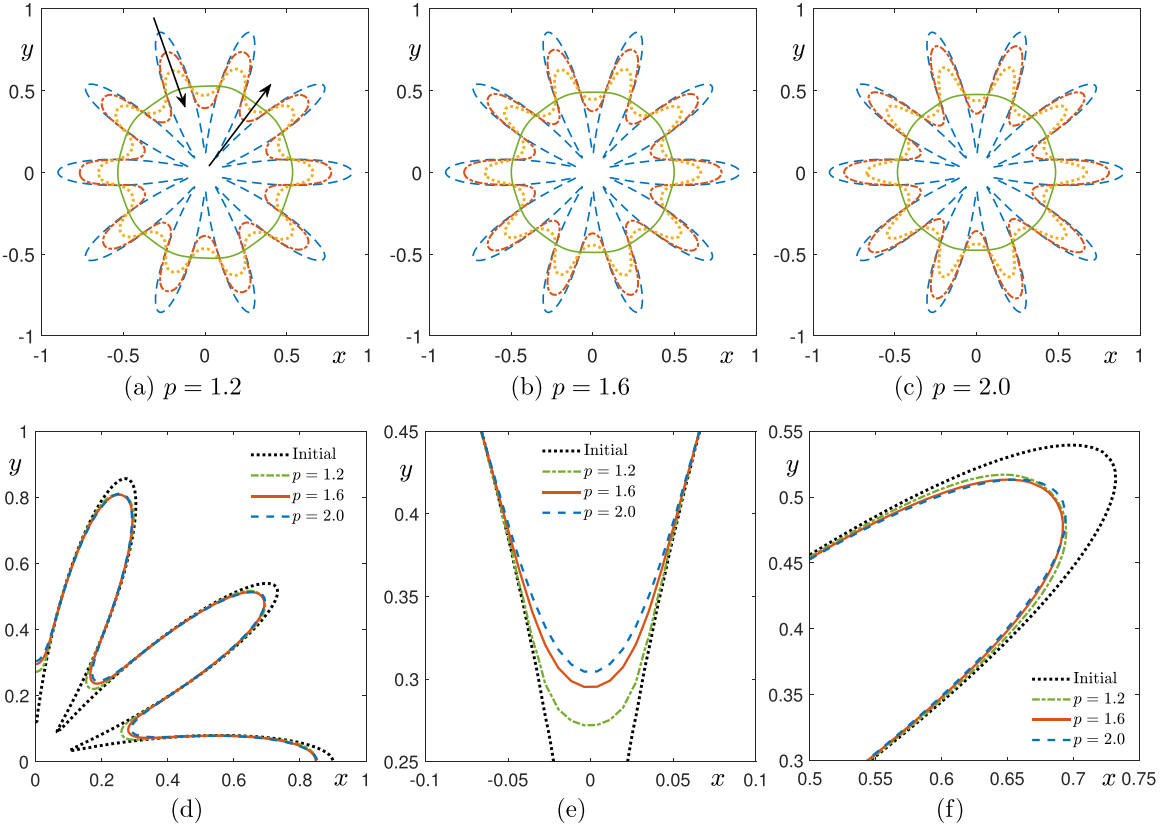


**Fig. 6.** (a)–(c) Evolution of numerical solutions according to  $p$  values: (a)  $p = 1.2$ , (b)  $p = 1.6$ , and (c)  $p = 2.0$ . (d)–(f) Comparison among the numerical solutions of the three different  $p$  values.

### 3.7. Effect of $p$ on the interfacial dynamics

We demonstrate the effect of  $p$  by observing the temporal evolution of two initially separated triangles on the computational domain  $\Omega = (0, 1)^2$ . Here, the parameters are used as  $N = 128$ ,  $h = 1/N$ ,  $\Delta t = 1.0 \times 10^{-4}$ , and  $\epsilon = 2 \times 10^{-2}$ . Figure 7 shows the temporal evolution of zero-level contour lines when two different  $p$  values, that is,  $p = 2.0$  and  $p = 1.6$  are used. When  $p = 2.0$ , the initially separated triangles are merged at an early evolutionary stage as shown in Fig. 7(a). In contrast, when  $p = 1.5$ , evolution occurs according to the mean curvature flow with the two triangles separated as shown in Fig. 7(b).

### 3.8. Comparison of $p$ -Laplacian and fractional Laplacian

First, we consider the early stage of evolution under three different equations, i.e., classical,  $p$ -Laplacian, and fractional AC equations. Recently, research on the fractional AC equation has been actively conducted because it can accurately describe anomalous diffusion phenomenon while satisfying the maximum principle [28–30]. To compare the evolution of the  $p$ -AC equation, the space-fractional AC equation [31,32] is given as follows:

$$\frac{du}{dt} = \epsilon \Delta^s u + \frac{1}{\epsilon} (u - u^3), \quad (10)$$

where  $s$  is the fractional order controlling the sharpness of the interface.

For the comparison, the random initial condition is given and the dynamics of phase separation in binary systems are observed. The computational domain is  $\Omega = (0, 1)^2$  and the parameters used are  $N = 256$ ,  $h = 1/N$ ,  $\Delta t = 5.0 \times 10^{-5}$ , and  $\epsilon = 3.0 \times 10^{-2}$ . Figure 8 shows five different phase separation dynamics corresponding  $p$ -AC equation  $p = 1.2$ ,  $p = 1.6$  on Eq. (3), and the classical AC equation i.e.  $p = 2.0$  (or  $s = 1.0$ ), and the fractional AC equation  $s = 0.9$ ,  $s = 0.6$  on Eq. (10). For this test, the fractional AC Eq. (10) is solved by employing the discrete cosine transform described in Appendix. We can observe that each morphological evolution has the coarsening kinetics, and all five cases share the phenomenon of spinodal decomposition in common. Furthermore, it seems that slow evolution occurs away from the center case  $p = 2.0$  and  $s = 1.0$ .

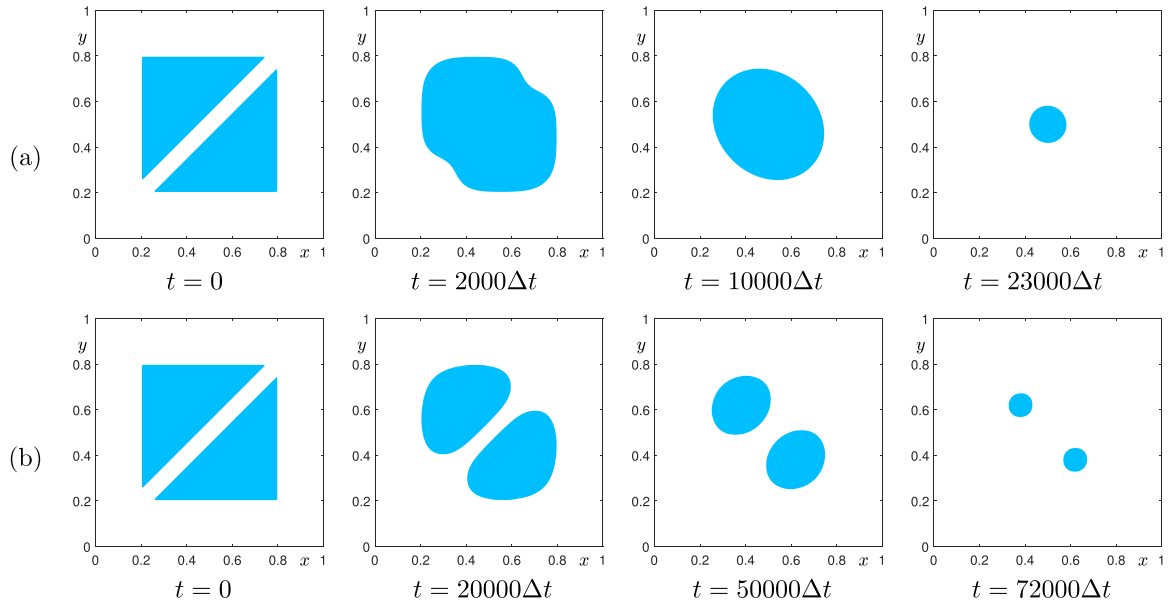


**Fig. 7.** Temporal evolution of zero-level contour lines when (a)  $p = 2.0$  and (b)  $p = 1.6$ . Each time is given below each column.

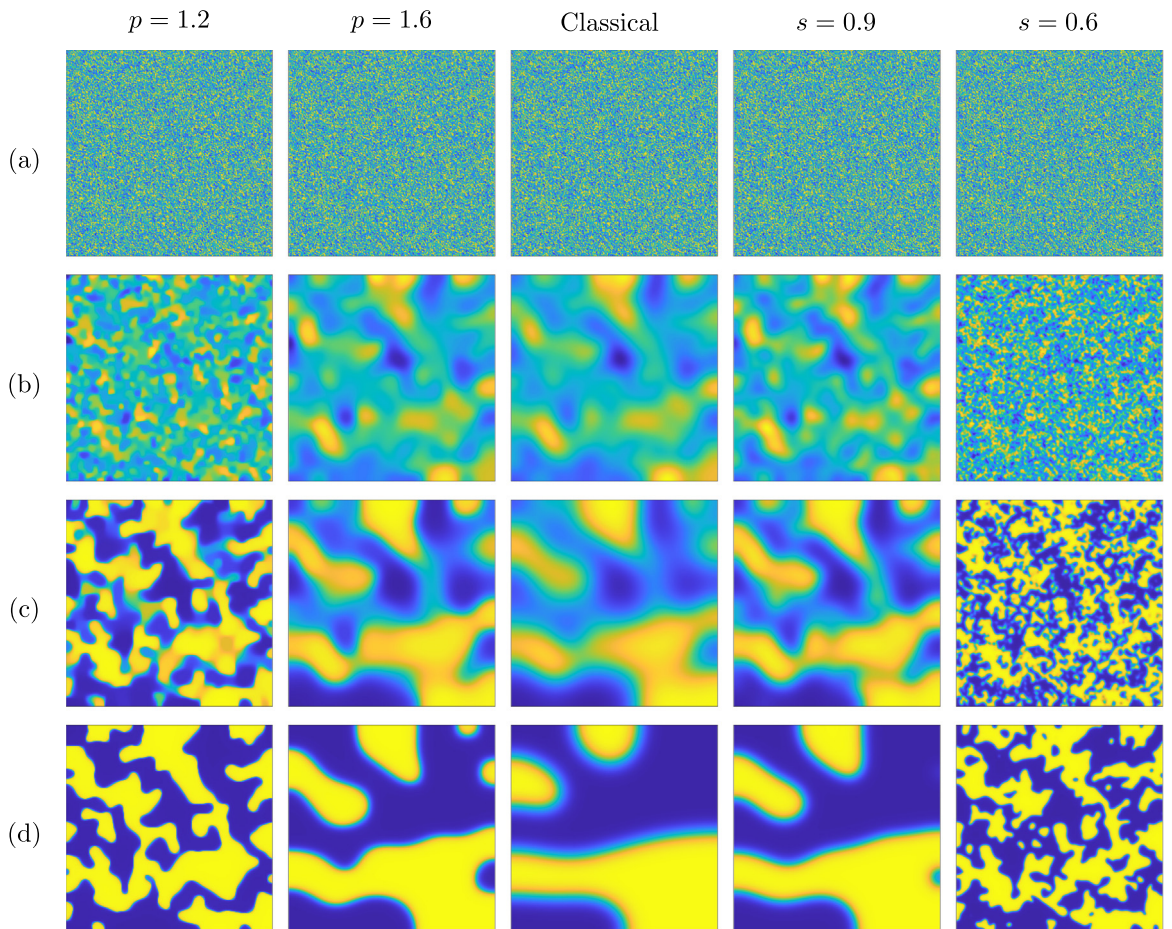


**Fig. 8.** Snapshots with respect to  $p$  and  $s$  values at (a)  $t = 0$ , (b)  $t = 1000\Delta t$ , (c)  $t = 3000\Delta t$ , and (d)  $t = 10000\Delta t$ . The values of  $p$  and  $s$  are written in the top row of each figure.

Second, we investigate the eigenvalues of three different Laplacian operators and their eigenvectors. Finding eigenvalues and eigenvectors of the  $p$ -Laplacian is an important issue but few cases have been studied, and it leads to an untractable problem. The 1D eigenvalues of the Neumann Laplacian  $-\Delta_h$  are given by

$$\lambda_i = \frac{4}{h^2} \sin^2\left(\frac{\pi(i-1)}{2N}\right) \quad \text{for } i = 1, \dots, N,$$

and corresponding eigenvectors for  $1 \leq j \leq N$  are

$$v_{j,i} = \begin{cases} \frac{1}{\sqrt{N}} & \text{for } i = 1, \\ \sqrt{\frac{2}{N}} \cos\left(\frac{\pi(i-1)(j-0.5)}{N}\right), & \text{otherwise.} \end{cases}$$

For simplicity, we set  $v_j = v_{j,i}$  for  $1 \leq i \leq N$ , then we define the eigenvectors by  $V := [v_1, \dots, v_N]$ . Now, the 1D fractional Laplacian with Neumann boundary conditions  $-\Delta_h^s$  can be approximated by

$$-\Delta_h^s = \sum_{i=1}^N (\lambda_i)^s v_i v_i^T.$$

The fractional Laplacian in a 2D domain can be constructed via the Kronecker sum of discrete Laplacian. Thus, we set the 2D fractional Laplacian  $-\Delta_{N,2}^s$  by

$$-\Delta_{h^2}^s = -\Delta_h^s \oplus -\Delta_h^s = -\Delta_h^s \otimes I_N + I_N \otimes -\Delta_h^s,$$

where  $I_N$  is the  $N \times N$  identity matrix.

The AC operator except that of nonlinear term, which induces phase separation, relates to the motion of the diffuse interface. Thus, to see the difference in interfacial dynamics, our concern is foremost about the Laplacian operators. We find the dominant eigenvalues and their eigenvectors of  $p$ -Laplacian numerically, and compare them with the eigenpair obtained from the classical Laplacian. In the phase-field model, binary regions are characterized by a scalar field, i.e., order parameter, which takes constant values in the bulk phase areas and varies continuously but radically across a diffuse front. It implies that two  $\pm 1$  bulk regions are not affected by the  $p$ -Laplacian operator since  $|\nabla u| = 0$  but only interfacial regions are highly dependent on  $|\nabla u|$ .

We present a numerical treatment based on the power method for finding eigenvalues and the gradient descent method for finding eigenvectors of Neumann  $p$ -Laplacian. Unlike the other eigenpair problems of the classical Laplacian, the form of eigenpairs for the  $p$ -Laplacian problem depends on the power of  $|\nabla u|$ , and is unknown as well. The power method for approximating eigenvalues iteratively calculates, and then their corresponding eigenvectors are found by the gradient descent method. Even though the power method is also applied to a symmetric matrix to determine the eigenvector, the gradient descent method gives us more robust and reliable updates for finding eigenvectors. Note that we see our operator  $\Delta_p$  to be a symmetric matrix, and allow repeated eigenvalues. For a good approximation of the dominant eigenvalues, our technique shifts all eigenvalues by subtracting  $\lambda_0 \in \mathbb{R}$  from the operator  $\Delta_p$ . Then we deflate  $\Delta_p$  repeatedly to approximate the next most dominant eigenvalue.

The power method is used to find a dominant eigenvalue, as follows. Let  $A := -\Delta_p + \lambda_0 I_{N^2} > 0$  be positive definite. For  $k \geq 0$  and by properly scaling the procedure given by

$$\begin{aligned} z^k &= Av^{k-1}, \\ v^k &= z^k / \|z^k\|, \\ \sigma^k &= (v^k)^T A v^k. \end{aligned}$$

We can find the approximated eigenvalue  $\sigma^k \approx \lambda$  as  $k$  increases. To find the corresponding eigenvector, let  $\sigma^\infty$  be the approximation of eigenvalue  $\lambda$  for large enough  $k$ , and set  $x^* \in \mathbb{R}^{N^2}$  be the corresponding eigenvector. This implies that we have  $F(\cdot) : \mathbb{R}^{N^2} \rightarrow \mathbb{R}$  defined by

$$x^* = \arg \min_x F(x), \quad \text{where } F(x) = \|Ax - \sigma^\infty x\|_2^2.$$

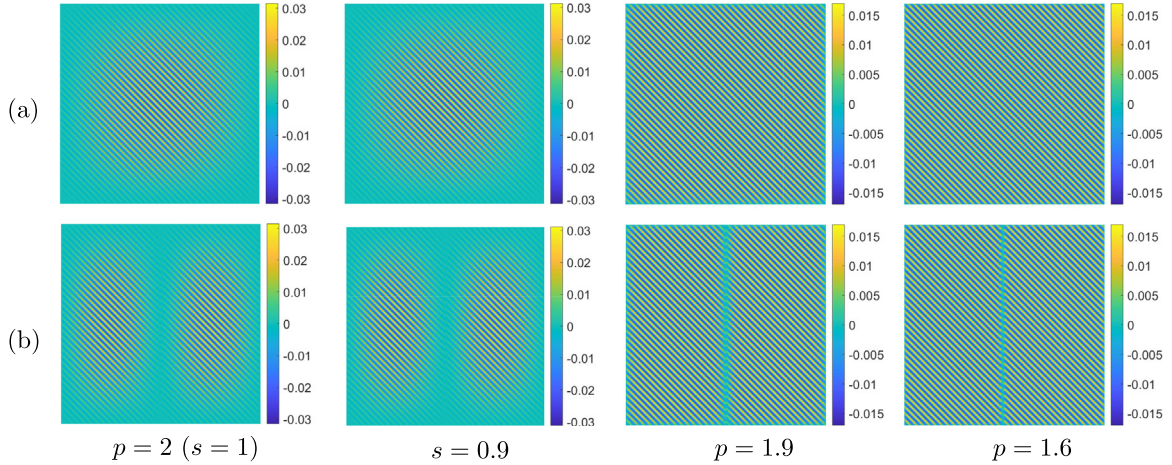
It is readily to see that  $F(x)$  is convex. For any  $\theta \in (0, 1)$  and  $x, y \in \mathbb{R}^{N^2}$ , we have

$$\begin{aligned} F(\theta x + (1 - \theta)y) &= \|A[\theta x + (1 - \theta)y] - \sigma^\infty[\theta x + (1 - \theta)y]\|_2^2 \\ &= \theta^2 F(x) + (1 - \theta)^2 F(y) + 2\theta(1 - \theta)x^T(A - \sigma^\infty I_{N^2})^2 y \\ &\leq \theta \|Ax - \sigma^\infty x\|_2^2 + (1 - \theta) \|Ay - \sigma^\infty y\|_2^2 \\ &= \theta F(x) + (1 - \theta)F(y), \end{aligned}$$

where the inequality follows that  $(A - \sigma^\infty I_{N^2})^2$  is positive semidefinite. Since  $F(x)$  is convex, we can find a unique solution of  $F(x)$ . For finding an accurate eigenvector, we present the gradient decent algorithm for minimizing the convex functional

**Table 1**First and second dominant eigenvalues according to  $p$  or  $s$  values.

Case	classical order	fractional		$p$ -Laplacian		
	$p = 2$ ( $s = 1$ )	$s = 0.9$	$s = 0.6$	$p = 1.9$	$p = 1.6$	$p = 1.2$
First	7.9952	3.0298	0.1649	7.4196	5.9936	4.2931
Second	7.9880	3.0273	0.1648	7.3807	5.9573	4.2891

**Fig. 9.** Eigenvectors of classical order ( $p = 2$  or  $s = 1$ ), fractional ( $s = 0.9$ ), and  $p$ -( $p = 1.9$  and  $p = 1.6$ ) Laplacian. (a) is the first dominant eigenvector and (b) is the second one.

$F(x)$ . The gradient of  $F$  is given by  $\nabla F(x) := 2(A^T A - 2\sigma^\infty A + (\sigma^\infty)^2)x$ . Then, the gradient descent method computes  $x^k$  with small step size  $\alpha > 0$ :

$$x^k = x^{k-1} - \alpha \nabla F(x), \quad \text{for } k \geq 0.$$

Now, let us observe the eigenvalues of  $-\Delta_p$  using the power method. We set the random initial condition on the computational domain  $\Omega = (0, 1)^2$  and take the parameters used are  $N = 64$  and  $h = 1/N$ . **Table 1** lists the eigenvalues and **Fig. 9** shows the first and second dominant eigenvectors of the classical order, fractional, and  $p$ -Laplacian, respectively. In **Table 1**, compared to the eigenvalues of the classical Laplacian, the eigenvalues decrease as the smaller  $s$  or  $p$  values are used. In the case of fractional Laplacian, it is confirmed that the eigenvectors are constant regardless of the  $s$  value as we mentioned above. For any values of  $s$  including  $s = 0.9$ , we obtain the same results as the eigenvectors of the classical order Laplacian, as shown in the first columns of **Fig. 9**. However, unlike the case of fractional Laplacian, it can be observed that the eigenvectors of  $p$ -Laplacian vary depending on the value of  $p$  and it is quite sensitive to the  $p$  values. In **Fig. 9**, it is observed that the values of the eigenvectors decrease as the value of  $p$  gets smaller. The second dominant eigenvectors of  $p = 1.9$  and  $p = 1.6$  show that the thickness of the interface becomes narrower when the smaller  $p$  is used.

#### 4. Conclusions

Phase-field modeling has been studied over the past decades, and different types of operators for the AC equations have been proposed and developed, hitherto. However, there are few results for the difference between the Laplacian operators (classical Laplacian, fractional Laplacian, and  $p$ -Laplacian) in the AC equation. Moreover, to the best of our knowledge, no other numerical studies have examined the behavior of the  $p$ -AC equation, compared to the classical or fractional AC equation. Therefore, we have analyzed a numerical scheme for the  $p$ -AC equation to confirm that the discrete solution also shares the boundedness and energy decay properties. We numerically demonstrated basic properties of the AC equation such as phase separation, boundedness of the solutions, and motion by mean curvature. Various computational tests were also performed to show the interfacial dynamics of AC equations and  $p$ -Laplacian. The advantage of the  $p$ -AC equation over the classical one is that sharpness of interface in evolutions can be adjusted to the  $p$  values. Moreover, we numerically investigated the eigenpairs of the  $p$ -Laplacian by comparing them with those of the classical and fractional Laplacian. From the numerical results, the eigenvectors depending on  $p$ -values are not constant but behaves differently compared to the fractional Laplacian and classical one.

In this paper, we have focused on examining the interfacial dynamics of  $p$ -AC equation. Since the  $p$ -AC equation that we consider is a second-order nonlinear partial differential equation on a 2D domain, the constraint on the time step size is not severe enough, therefore, we simply have employed the explicit scheme and we could have the boundedness of a solution and energy decay properties. However, when it comes to the implicit scheme for the  $p$ -AC equation given above, we find it difficult to analyze the term  $|\nabla u|$  in the  $p$ -AC equation because of its non-linearity. In future work, we would like to investigate the implicit type scheme for the  $p$ -AC equation and the convergence analysis. In addition, if we simultaneously consider the worst theoretical condition over both the boundedness and energy decay properties, it is too strict for analysis. For practical purposes, we can consider the condition which is not the worst. However, it is worth discussing the assumptions for the boundedness and energy dissipation properties. Nevertheless, we need a much more complicated analysis for the properties. Therefore, we will continue the analysis in subsequent work.

## Data availability

No data was used for the research described in the article.

## Acknowledgment

The first author (D. Lee) acknowledges support from the National Research Foundation of Korea (NRF-2018R1D1A1B07049292). The corresponding author(C. Lee) was supported by the National Research Foundation of Korea(NRF) grant funded by the Korea government(MSIT) (NRF-2022R1C1C2003896).

For the given data  $\{u_{m,n}^k \mid m = 1, \dots, M \text{ and } n = 1, \dots, N\}$ , the discrete cosine transform is defined.

$$\hat{u}_{q,r}^k = \alpha_q \beta_r \sum_{m=1}^M \sum_{n=1}^N u_{m,n}^k \cos \frac{(2m-1)(q-1)\pi}{2M} \cos \frac{(2n-1)(r-1)\pi}{2N},$$

for  $q = 1, \dots, M$  and  $r = 1, \dots, N$ , where,

$$\alpha_p = \begin{cases} \sqrt{1/M}, & p = 1 \\ \sqrt{2/M}, & 2 \leq p \leq M \end{cases} \quad \text{and} \quad \beta_r = \begin{cases} \sqrt{1/N}, & r = 1 \\ \sqrt{2/N}, & 2 \leq r \leq N \end{cases}$$

For simplicity, we denote some variables by

$$x_m = \frac{(2m-1)L_x}{2M}, \quad y_n = \frac{(2n-1)L_y}{2N}, \quad \xi_q = \frac{q-1}{L_x}, \quad \eta_r = \frac{r-1}{L_y}.$$

By using these variables, we obtain the discrete cosine transform:

$$\hat{u}_{q,r}^k = \alpha_q \beta_r \sum_{m=1}^M \sum_{n=1}^N u_{m,n}^k \cos(x_m \pi \xi_q) \cos(y_n \pi \eta_r).$$

The inverse discrete cosine transform is

$$u_{m,n}^k = \sum_{q=1}^M \sum_{r=1}^N \alpha_q \beta_r \hat{u}_{q,r}^k \cos(\xi_q \pi x_m) \cos(\eta_r \pi y_n). \quad (11)$$

Let us assume that

$$u(x, y, k\Delta t) = \sum_{q=1}^M \sum_{r=1}^N \alpha_q \beta_r \hat{u}_{q,r}^k \cos(\xi_q \pi x) \cos(\eta_r \pi y).$$

The  $x$  and  $y$  second-order partial derivatives translate into analytical differentiation of the exponentials.

$$\frac{\partial^2 u}{\partial x^2}(x, y, k\Delta t) = - \sum_{q=1}^M \sum_{r=1}^N (\xi_q \pi)^2 \alpha_q \beta_r \hat{u}_{q,r}^k \cos(\xi_q \pi x) \cos(\eta_r \pi y),$$

$$\frac{\partial^2 u}{\partial y^2}(x, y, k\Delta t) = - \sum_{q=1}^M \sum_{r=1}^N (\eta_r \pi)^2 \alpha_q \beta_r \hat{u}_{q,r}^k \cos(\xi_q \pi x) \cos(\eta_r \pi y).$$

Then, the Laplacian operator is defined as

$$\Delta u(x, y, k\Delta t) = - \sum_{q=1}^M \sum_{r=1}^N [(\xi_q \pi)^2 + (\eta_r \pi)^2] \alpha_q \beta_r \hat{u}_{q,r}^k \cos(\xi_q \pi x) \cos(\eta_r \pi y).$$

We apply the explicit Euler scheme to Eq. (10).

$$\frac{u_{i,j}^{k+1} - u_{i,j}^k}{\Delta t} = \epsilon \Delta^s u_{i,j}^k + \frac{u_{i,j}^k - (u_{i,j}^k)^3}{\epsilon} \quad (12)$$

Thus, Eq. (12) can be transformed into the discrete cosine space as follows:

$$\frac{\hat{u}_{q,r}^{k+1} - \hat{u}_{q,r}^k}{\Delta t} = -\epsilon \{(\xi_q \pi)^2 + (\eta_r \pi)^2\}^s \hat{u}_{q,r}^k + \frac{\hat{u}_{q,r}^k - \widehat{(u_{q,r}^k)^3}}{\epsilon}.$$

Therefore, we obtain the following discrete cosine transform

$$\hat{u}_{q,r}^{k+1} = \hat{u}_{q,r}^k - \Delta t \epsilon \{(\xi_q \pi)^2 + (\eta_r \pi)^2\}^s \hat{u}_{q,r}^k + \Delta t \frac{\hat{u}_{q,r}^k - \widehat{(u_{q,r}^k)^3}}{\epsilon}.$$

The corresponding function  $u_{m,n}^{k+1}$  can be computed using Eq. (11).

## References

- [1] J.G. Azorero, I.P. Alonso, Existence and nonuniqueness for the  $p$ -Laplacian, *commun. Partial Differ. Equ.* 12 (12) (1987) 1389–1430.
- [2] P. Drábek, S.I. Pohozaev, Positive solutions for the  $p$ -Laplacian: application of the fibering method, *Proc. R. Soc. Edinb. A.* 127 (4) (1997) 703–726.
- [3] W. Allegretto, Y. XiHuang, A Picone's identity for the  $p$ -Laplacian and applications, *Nonlinear Anal. Theory Methods Appl.* 32 (7) (1998) 819–830.
- [4] A. Lê, Eigenvalue problems for the  $p$ -Laplacian, *Nonlinear Anal. Theory Methods Appl.* 64 (5) (2006) 1057–1099.
- [5] O. Bazighifan, On the oscillation of certain fourth-order differential equations with  $p$ -Laplacian like operator, *Appl. Math. Comput.* 386 (2020) 125475.
- [6] T. Bühlér, M. Hein, Spectral clustering based on the graph  $p$ -Laplacian, in: Proceedings of the 26th Annual International Conference on Machine Learning, 2009, pp. 81–88.
- [7] A. Elmoataz, X. Desquesnes, O. Lézoray, Non-local morphological PDEs and  $p$ -laplacian equation on graphs with applications in image processing and machine learning, *IEEE J. Sel. Top. Signal Process.* 6 (7) (2012) 764–779.
- [8] Y.S. Lee, S.Y. Chung, Extinction and positivity of solutions of the  $p$ -Laplacian evolution equation on networks, *J. Math. Anal. Appl.* 386 (2) (2012) 581–592.
- [9] J.H. Kim, J.H. Park, Complete characterization of flocking versus nonflocking of Cucker-Smale model with nonlinear velocity couplings, *Chaos Solitons Fractals* 13 (4) (2020) 109714.
- [10] J. Liu, Boundedness in a chemotaxis-(Navier-) Stokes system modeling coral fertilization with slow  $p$ -Laplacian diffusion, *J. Math. Fluid Mech.* 22 (1) (2020) 10.
- [11] G.A. Zou, X. Wang, T.W. Sheu, Finite element analysis of a new phase field model with  $p$ -Laplacian operator, *Math. Comput. Simul.* 185 (2021) 134–152.
- [12] S.N. Antonsev, K. Khompysh, Kelvin-Voight equation with  $p$ -Laplacian and damping term: existence, uniqueness and blow-up, *J. Math. Anal. Appl.* 446 (2) (2017) 1255–1273.
- [13] W. Feng, A.J. Salgado, C. Wang, S.M. Wise, Preconditioned steepest descent methods for some nonlinear elliptic equations involving  $p$ -Laplacian terms, *J. Comput. Phys.* 334 (2017) 45–67.
- [14] J. Shen, C. Wang, X. Wang, S.M. Wise, Second-order convex splitting schemes for gradient flows with Ehrlich-Schwoebel type energy: application to thin film epitaxy, *SIAM J. Numer. Anal.* 50 (1) (2012) 105–125.
- [15] S.M. Allen, J.W. Cahn, A microscopic theory for antiphase boundary motion and its application to antiphase domain coarsening, *Acta Metall.* 27 (6) (1979) 1085–1095.
- [16] M. Beneš, V. Chalupecký, K. Mikula, Geometrical image segmentation by the Allen–Cahn equation, *Appl. Numer. Math.* 51 (2–3) (2004) 187–205.
- [17] J. Zhang, C. Chen, X. Yang, A novel decoupled and stable scheme for an anisotropic phase-field dendritic crystal growth model, *Appl. Math. Lett.* 95 (2019) 122–129.
- [18] D. Lee, J. Kim, Mean curvature flow by the Allen–Cahn equation, *Eur. J. Appl. Math.* 26 (4) (2015) 535–559.
- [19] Y. Li, S. Guo, Triply periodic minimal surface using a modified Allen–Cahn equation, *Appl. Math. Comput.* 295 (2017) 84–94.
- [20] C. Wang, X. Wang, S.M. Wise, Unconditionally stable schemes for equations of thin film epitaxy, *Discret. Contin. Dyn. Syst.* 28 (1) (2010) 405.
- [21] Z. Qiao, C. Wang, S.M. Wise, Z. Zhang, Error analysis of a finite difference scheme for the epitaxial thin film model with slope selection with an improved convergence constant, *Int. J. Numer. Anal. Model.* 14 (2) (2017) 283–305.
- [22] W. Feng, C. Wang, S.M. Wise, Z. Zhang, A second-order energy stable backward differentiation formula method for the epitaxial thin film equation with slope selection, *Numer. Meth. Part. Differ. Equ.* 34 (6) (2018) 1975–2007.
- [23] S. Wang, W. Chen, H. Pan, C. Wang, Optimal rate convergence analysis of a second order scheme for a thin film model with slope selection, *J. Comput. Appl. Math.* 377 (2020) 112855.
- [24] K. Cheng, C. Wang, S.M. Wise, An energy stable BDF2 fourier pseudo-spectral numerical scheme for the square phase field crystal equation, *Commun. Comput. Phys.* 26 (5) (2019) 1335–1364.
- [25] M. Wang, Q. Huang, C. Wang, A second order accurate scalar auxiliary variable (SAV) numerical method for the square phase field crystal equation, *J. Sci. Comput.* 88 (2021) 33.
- [26] Q. Cheng, C. Wang, Error estimate of a second order accurate scalar auxiliary variable (SAV) numerical method for the epitaxial thin film equation, *Adv. Appl. Math. Mech.* 13 (2021) 1318–1354.
- [27] I. Cohen, A. Falik, G. Gilboa, Stable explicit  $p$ -Laplacian flows based on nonlinear eigenvalue analysis, in: In International Conference on Scale Space and Variational Methods in Computer Vision, Springer, Cham, 2019, pp. 315–327.

- [28] F. Song, C. Xu, G.E. Karniadakis, A fractional phase-field model for two-phase flows with tunable sharpness: algorithms and simulations, *Comput. Meth. Appl. Mech. Eng.* 305 (2016) 376–404.
- [29] Z. Li, H. Wang, D. Yang, A space-time fractional phase-field model with tunable sharpness and decay behavior and its efficient numerical simulation, *J. Comput. Phys.* 347 (2017) 20–38.
- [30] H. Zhang, J. Yan, X. Qian, X. Gu, S. Song, On the preserving of the maximum principle and energy stability of high-order implicit-explicit Runge–Kutta schemes for the space-fractional Allen–Cahn equation, *Numer. Algorithms* 88 (2021) 1309–1336.
- [31] S. Lee, D. Lee, The fractional Allen–Cahn equation with the sextic potential, *Appl. Math. Comput.* 351 (2019) 176–192.
- [32] F. Achleitner, C. Kuehn, J.M. Melenk, A. Rieder, Metastable speeds in the fractional Allen–Cahn equation, *Appl. Math. Comput.* 408 (2021) 126329.